Application of Crossover Theory to the SAFT-VR Equation of State: SAFT-VRX for Pure Fluids

Clare McCabe* and Sergei B. Kiselev

Department of Chemical Engineering, Colorado School of Mines, Golden, Colorado 80401

The molecular-based SAFT equation of state has proven to be very versatile in the prediction of fluid phase equilibria. However, in common with all analytic equations of state, SAFT exhibits classical behavior in the critical region rather than the nonanalytical, singular behavior seen in real fluids. As a result, accurate agreement over the whole phase diagram cannot be obtained and must be localized to either the critical or subcritical regions. To overcome this problem, we have combined the SAFT-VR equation of state with a crossover technique developed by Kiselev (Kiselev, S. B. *Fluid Phase Equilib.* **1998**, *147*, 7) to obtain the SAFT-VRX equation. We have applied SAFT-VRX to both associating and nonassociating pure fluids. Results are presented for *n*-alkanes, water, and carbon dioxide. Furthermore, by fitting to the phase diagram and PVT behavior for a small number of *n*-alkanes, we have developed simple expressions for the potential model parameters for the *n*-alkane homologous series. These prescriptions enable the accurate prediction of the thermodynamic properties, including the phase diagram, of *n*-alkanes without additional fitting to experimental data. Additionally, by combining density functional theory with SAFT-VRX we predict the surface tension of both low and high molecular weight *n*-alkanes.

I. Introduction

Since the pioneering work of van der Waals on the first molecular theory of fluids, the development of accurate equations of state firmly based in statistical mechanics continues to be an active area of research. While early equations of state were predominantly empirical, advances in statistical theory, computational power, and molecular simulation algorithms have enabled the development of equations of state based on molecular principles, often using insights gained from molecular simulation to improve the underlying model. However, despite these advances, the goal of accurately describing fluid phase behavior in the critical region, without compromising the region of the phase diagram away from the critical point, remains elusive.

van der Waals derived his equation of state from the ideal gas equation by introducing corrections for both the nonzero size of the molecules and the attractive interactions between them. For the latter, it was assumed that every molecule interacts with the others in the fluid through an average (or mean) field created by the attractive interactions of all the other molecules, in what is nowadays termed the mean field approximation. Many engineering equations of state, such as the Peng−Robinson[1] or Redlich−Kwong[2] equations and their variants,[3] are based on the van der Waals equation, with modifications being made to the treatment of the hard sphere repulsive term and/or the mean field attractive term (usually the latter). Fitted to experimental data, such equations have been successful in describing fluids composed of simple molecules, such as noble gases and simple organic (e.g., CH_4, C_2H_6) and inorganic (e.g., N_2) compounds. The treatment of more complex systems with these equations of state, such as heavy hydrocarbon molecules and hydrogen-bonding fluids, usually involves the introduction of additional ad hoc parameters, since the original equations of state have not been derived from a theoretical basis that accommodates such complexity. In particular, these semiempirical equations of state do not take into account in any rigorous way molecular shape and molecular association. Accounting for the latter has figured prominently in recent efforts to develop equations of state. For example, the perturbed hard chain theory (PHCT),[4,5] the associating perturbed anisotropic chain theory (APCAT),[6] and their variants[3,7] have been widely used to correlate experimental data, but in common with the simpler cubic equations of state they have limited predictive value far away from the systems and state conditions to which the model parameters were fitted.

Molecular-based equations of state provide a framework in which the effects of molecular shape and interactions on the thermodynamic properties can be separated and quantified. Each contribution depends on molecular parameters that have a real physical meaning, such as the size of the molecule or the functional groups comprising it, and in principle do not depend on the thermodynamic conditions. The statistical associating fluid theory (SAFT) is one such equation of state that was proposed in the late 1980s by Chapman and co-workers on the basis of the thermodynamic perturbation theory of Werthiem.[8−11] An important feature of SAFT is that it explicitly takes into account nonsphericity and association interactions and provides a powerful and successful method for studying the phase behavior of chain molecules, both nonassociating and associating. SAFT was originally developed[12,13] to model associating fluids as chains of Lennard-Jones segments with association sites, though there have been many variations on the original expressions in recent years (see the excellent review by Muller and Gubbins[14]). The simplest version of SAFT describes chains of associating hard-sphere (HS) segments with attractive interactions

* To whom correspondence should be addressed. E-mail: cmccabe@mines.edu.

10.1021/ie034288n CCC: $27.50
Published on Web 04/30/2004

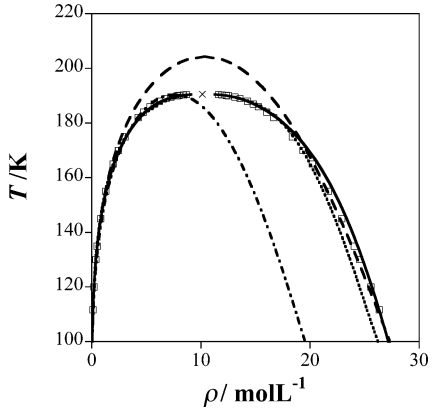

Figure 1. Coexisting liquid and gas densities for methane from SAFT-VRX (—), SAFT-VR (- - -), SAFT-VR with rescaled parameters (— · —), and crossover HR-SAFT[42] (···) compared with experimental data[74] (symbols).

described at the van der Waals mean-field level (SAFT-HS).[15,16] SAFT-HS has been used successfully to study systems with strong association such as the high-pressure critical lines of mixtures of alkanes and water,[17] and mixtures containing hydrogen fluoride.[18] At a similar level of theory is the most extensively applied version of SAFT, that of Huang and Radosz[19,20] (henceforth denoted HR-SAFT), which been used to correlate the phase behavior of a wide range of fluid systems. More recently, the SAFT approach has been extended to describe chain molecules formed from hard-core monomers with attractive potentials of variable range (SAFT-VR).[21,22] This version of the theory provides an additional parameter, λ, which characterizes the range of the attractive part of the potential and significantly improves upon the van der Waals mean-field treatment used in the SAFT-HS approach. The chain contribution is also improved by using the contact values of the distribution function for the actual monomers instead of those for the HS reference system. In previous work, SAFT-VR has been used to accurately describe the phase behavior of a wide range of industrially important substances and their mixtures (see, for example, refs 23−30). In particular, the phase behavior of hydrocarbon systems has been extensively studied.[23,25,27] Although these systems display relatively simple phase behavior (typically type I in the scheme of Scott and van Konynenburg[31]), they provide a good testing ground for a new theory, and we shall briefly consider these systems in more detail[23−25,27,30] as they highlight the shortcomings of SAFT-VR in the critical region.

In the description of pure component phase behavior, the SAFT-VR potential parameters are determined by fitting to experimental saturated liquid density and vapor pressure data. The result of such a fitting procedure for methane is shown in Figure 1 and clearly illustrates the overprediction of the critical point, which is a direct result of the classical behavior of SAFT-VR in the critical region and is seen for all engineering equations of state that are analytical in the free energy. When the critical region is of interest the optimized parameters can be rescaled to the experimental critical temperature (T_c) and pressure (P_c); however, agreement with the critical point comes at the cost of a poorer prediction at low temperatures and pressures. Despite these limitations, the application of SAFT-VR to mixtures has led to some extraordinary successes. For example, using the pure-fluid rescaled parameters and the unlike (or cross) interaction parameters obtained from simple Lorentz−Berthelot combining rules, we were able to obtain excellent agreement between the predictions of the SAFT-VR equation of state (EOS) and experimental data for the pure light *n*-alkanes and the critical lines of their binary mixtures without fitting to any binary mixture data.[25] Furthermore, we were able to predict even very subtle features of the phase diagram, such as the transition from type I to type V phase behavior observed for the methane + *n*-hexane binary mixture, again without fitting to any binary mixture data.[23] We have also applied SAFT-VR to high molecular weight hydrocarbons,[27] thus demonstrating the suitability of the SAFT approach to study long chain molecules. Furthermore, we obtained linear relations between the potential model parameters and carbon number, making the SAFT-VR parameters transferable to alkanes of any molecular weight. However, while rescaling the pure component parameters to the experimental critical point works well for the light hydrocarbons and enabled the accurate prediction of the high-pressure critical lines, rescaling results in significant deviations from experimental data at lower temperatures and pressures, and for the liquid densities (Figure 1).

Table 1. Definitions and Values of the Major Critical Exponents in the Mean-Field (MF) and Scaling (SC) Theory[a,32]

exponent	quantity	MF	SC
α	$C_v \sim (T - T_c)^{-\alpha}$, $\rho = \rho_c$	0	0.112 ± 0.003
β	$\rho_l - \rho_v \sim (T_c - T)^{\beta}$, $T \rightarrow T_c^-$	0.5	0.325 ± 0.002
γ	$K_T \sim \lvert T - T_c\rvert^{-\gamma}$, $\rho = \rho_c$	1	1.239 ± 0.002
δ	$P - P_c \sim (\rho - \rho_c)\lvert\rho - \rho_c\rvert^{\delta} - 1$, $T = T_c$	3	4.8 ± 0.02

[a] The quantities K_T and C_V are the isothermal compressibility and isochoric specific heat, respectively.

Near the critical point, thermodynamic behavior is described by nonanalytic scaling laws, with universal scaling functions and universal critical exponents.[32] While equations of state such as SAFT provide accurate descriptions of phase behavior far from the critical region, as noted earlier, they fail close to it, predicting mean field critical behavior, rather than that observed experimentally which is consistent with the universality class of the 3-dimensional Ising model.[33] While the inclusion of more accurate effective potentials, such as the Lennard-Jones or square-well potentials, improves the description of the short range, local structure, the resulting equations of state are still mean field theories at long range as they neglect the long-ranged density fluctuations which exceed the potential model interactions and therefore are not accounted for by classical equations of state. Hence, like essentially all other engineering equations of state, SAFT-VR, being a mean field theory, exhibits the classical critical exponents given in Table 1, leading to a parabolic coexistence curve in the critical region ($T_c - T \sim (\rho_l - \rho_v)^2$, $T \rightarrow T_c^-$, or $\rho_l - \rho_v \sim (T_c - T)^{\beta}$, $T \rightarrow T_c^-$, with $\beta = 0.5$, where ρ_l and ρ_v are the densities of the coexisting liquid (l) and vapor (v) phases and β is the critical exponent characterizing the shape of the coexistence curve in the vicinity of the critical point) compared to the exact experimental behavior ($\beta = 0.325 \pm 0.002$).[32] Although the asymptotic scaling laws are observed in pure fluids only extremely close to its critical point at $|\tau| \ll Gi$ (where $\tau = T/T_c - 1$ is a reduced temperature and Gi is the Ginzburg number), at $Gi \leq |\tau| < 1$ the critical fluctuations also

affect the thermodynamic properties of fluids in a substantial range of densities around the critical point.[34,35]

An accurate thermodynamic description of the global fluid phase diagram is possible through a so-called crossover EOS which satisfies not only the asymptotic critical power laws, but also incorporates crossover to regular thermodynamic behavior far from the critical point. The earliest crossover EOS, developed by Chapela and Rowlinson,[36] consisted of summing the scaling and analytic functions weighted by a switching function which suppressed the analytic function near the critical point and the scaling function away from the critical point. However, this and other early approaches based on empirical crossover functions suffered from discontinuities in the crossover region.[33] A theoretical approach to crossover behavior based on the fundamental results of the renormalization group theory was developed by Sengers and co-workers[37−39] and by Kiselev et al.[40−42] More rigorous than the Chapela−Rowlinson method, this approach usually begins at the critical point of the fluid and then describes how the asymptotic Ising model becomes modified on moving away from the critical point. Such crossover treatments have been applied to simple semiempirical equations of state (see for example refs 40, 41, 43, 44) and to simpler versions of the SAFT EOS.[41,44−48] In this earlier work on crossover SAFT models, the expressions of Huang and Radosz (HR-SAFT)[19] have been used in combination with Kiselev's crossover method. Since SAFT-VR provides a much more rigorous and accurate description of the thermodynamic behavior away from the critical point, we anticipate that the resulting crossover equation of state, SAFT-VRX, will provide a superior description of the entire fluid phase region. An alternative crossover approach was proposed by White and Zhang,[49,50] and used by Jiang and Prausnitz in the development of a crossover EOS for chain molecules (EOSCF +RG).[51−53] This crossover EOS has been used to determine the critical properties of hydrocarbons and their binary mixtures, though in its present formulation associating systems cannot be studied. Furthermore, the crossover method used can only be solved numerically and so the resulting equation of state is not in a closed form, unlike SAFT-VRX.

The remainder of the paper is organized as follows. In section II, we describe the SAFT-VR equation of state with the modification proposed by Patel and Galindo to describe square-well potentials of variable range beyond $\lambda = 1.8$.[54] In section III, we present the SAFT-VRX equation of state for associating chain fluids. Results for the thermodynamic and phase behavior of pure fluids are presented in section IV and compared with the original SAFT-VR equation, a crossover description of the HR-SAFT equation, and experiment. In section V, concluding remarks are made, and future work is discussed.

II. SAFT-VR

Within the SAFT framework, following the seminal work of Wertheim, the dimensionless Helmholtz free energy $a = A/NkT$ for a fluid of associating chain molecules is written as a sum of the separate contributions to the free energy, viz.

$$a = a^{\text{ideal}} + a^{\text{mono}} + a^{\text{chain}} + a^{\text{assoc}} \tag{1}$$

where N is the total number of molecules, T the temperature, and k the Boltzmann constant. a^{ideal} is the ideal free energy, a^{mono} the contribution to the free energy due to the monomeric segments, a^{chain} the contribution due to the formation of a chain of m monomers, and a^{assoc} the contribution due to association.

The ideal contribution to the free energy is given by

$$a^{\text{ideal}} = \ln(\rho\Lambda^3) - 1 \tag{2}$$

where $\rho = N/V$ is the number density of chain molecules, N the number of molecules, V the volume of the system, and Λ the thermal de Broglie wavelength. Since we separate out the ideal term, we note the remaining terms are residual free energies.

We can express the monomer Helmholtz free energy in terms of the free energy per monomer a^{M}

$$a^{\text{mono}} = m\frac{A^{\text{M}}}{N_s kT} = ma^{\text{M}} \tag{3}$$

where m is the number of spherical monomer segments which make up each chain and N_s is the total number of monomer segments. Using the Barker and Henderson perturbation theory with a hard-sphere reference system, the monomer free energy per segment is obtained from the expansion

$$a^{\text{M}} = a^{\text{HS}} + \beta a_1 + \beta^2 a_2 \tag{4}$$

where $\beta = 1/kT$. The quantity a^{HS} describes the contribution to the free energy due to the repulsive interactions between the molecular cores, and a_1 and a_2 are the first and second perturbation terms associated with the attractive energy. The expression of Carnahan and Starling is used for the reference hard-sphere term

$$a^{\text{HS}} = \frac{4\eta - 3\eta^2}{(1-\eta)^2} \tag{5}$$

where η is the packing fraction. The mean attractive energy given by the first perturbative term corresponds to the average of the monomer−monomer interaction energy calculated with the hard sphere structure. In this work, the attractive perturbation is described by a square-well potential

$$u(r) = \begin{cases} +\infty & \text{if } r < \sigma \\ -\epsilon & \text{if } \sigma \le r < \lambda\sigma \\ 0 & \text{if } r > \lambda\sigma \end{cases} \tag{6}$$

Using the mean-value theorem we can obtain an expression for a_1 in terms of an effective packing fraction η_{eff} evaluated at contact,[21] giving

$$a_1 = -4\eta\epsilon(\lambda^3 - 1)g^{\text{HS}}(\sigma, \eta_{\text{eff}}) \tag{7}$$

where the Carnahan and Starling equation of state is used to evaluate $g^{\text{HS}}(\sigma, \eta_{\text{eff}})$. In the original SAFT-VR approach the dependence of the effective packing fraction η_{eff} on the actual packing fraction η and the potential range λ was described for $\lambda = 1.1-1.8$ by a polynomial parametrization of the formwhere the coef-

$$\eta_{\text{eff}}(\eta, \lambda) = c_1\eta + c_2\eta^2 + c_3\eta^3 \tag{8}$$

ficients c_n are given by

$$\begin{pmatrix} c_1 \\ c_2 \\ c_3 \end{pmatrix} = \begin{pmatrix} 2.25855 & -1.50349 & 0.249434 \\ -0.669270 & 1.40049 & -0.827739 \\ 10.1576 & -15.0427 & 5.30827 \end{pmatrix} \begin{pmatrix} 1 \\ \lambda \\ \lambda^2 \end{pmatrix} \quad (9)$$

In the nonlinear regression analysis applied during this work for the optimization of the SAFT-VRX EOS, the upper limit on λ led to unphysical values of the parameters and the divergence of the optimization procedure. In recent work, Patel et al.[54] have examined other functional forms for η_{eff} in order to increase the applicable range of λ to 3. Therefore, in this work we have used the Pade expression proposed by Patel et al., viz.

$$\eta_{\text{eff}}(\eta, \lambda) = \frac{c_1\eta + c_2\eta^2}{(1 + c_3\eta)^3} \quad (10)$$

with coefficients

$$\begin{pmatrix} c_1 \\ c_2 \\ c_3 \end{pmatrix} = \begin{pmatrix} -3.16492 & 13.35007 & -14.80567 & 5.07286 \\ 43.00422 & -191.66232 & 273.89683 & -128.93337 \\ 65.04194 & -266.46273 & 361.04309 & -162.69963 \end{pmatrix} \begin{pmatrix} 1/\lambda \\ 1/\lambda^2 \\ 1/\lambda^3 \\ 1/\lambda^4 \end{pmatrix} \quad (11)$$

The second perturbation term a_2 describes the fluctuation of the attractive energy as a consequence of the compression of the fluid by the action of the attractive well and is written in terms of a_1 within the local compressibility approximation

$$a_2 = \frac{1}{2}K^{\text{HS}}\epsilon\rho_s\frac{\partial a_1}{\partial \rho_s} \quad (12)$$

where K^{HS} is the hard-sphere isothermal compressibility of Percus−Yevick

$$K^{\text{HS}} = \frac{(1-\eta)^4}{1 + 4\eta + 4\eta^2} \quad (13)$$

The contribution to the free energy due to chain formation from m monomer segments is expressed as

$$a^{\text{chain}} = -(m-1)\ln y^{\text{SW}}(\sigma) \quad (14)$$

where the contact value of the monomer−monomer background correlation function is given by

$$y^{\text{SW}}(\sigma) = g^{\text{SW}}(\sigma)\exp(-\beta\epsilon) \quad (15)$$

which is obtained from the high-temperature expansion of $g^{\text{SW}}(\sigma)$

$$g^{\text{SW}}(\sigma) = g^{\text{HS}}(\sigma) + \beta\epsilon g_1(\sigma) \quad (16)$$

where $g_1(\sigma)$ can be obtained from the pressure expression (the Clausius virial theorem) and the first derivative of the free energy with respect to the density (see ref 21). Finally, the free energy due to association is given by

$$a^{\text{assoc}} = \left[\sum_{a=1}^{n}\left(\ln X_a - \frac{X_a}{2}\right) + \frac{n}{2}\right] \quad (17)$$

where the sum is over all sites a on the model molecule and X_a is the fraction of molecules not bonded at site a and is given by the mass action equation

$$X_a = \frac{1}{1 + \sum_{b=1}^{n}\rho X_b\Delta_{a,b}} \quad (18)$$

Here $\Delta_{a,b}$ characterizes the association between site a and b on different molecules and is given by

$$\Delta_{a,b} = K_{a,b}f_{a,b}g^{\text{M}}(\sigma) \quad (19)$$

where $K_{a,b}$ is the volume available for bonding (determined from the position and range of the bonding site), and $f_{a,b}$ is the Mayer f-function for the $a-b$ site−site interaction given by $f_{a,b} = \exp(u_{ab}/kT) - 1$ where $u_{a,b}$ describes the strength of the site−site interaction.[16]

III. SAFT-VRX Equation

In deriving a crossover SAFT-VR equation (SAFT-VRX), which reproduces the scaling laws in the critical region and far away from the critical point is transformed into the original SAFT-VR equation, we use the crossover approach developed by Kiselev.[40] Following this approach, one needs to start from the full analytical expression for the thermodynamic potential given by eq 1, rewritten in the form

$$a(T, v) = a^{\text{res}}(T, v) + a^{\text{ideal}}(T, v) \quad (20)$$

where $a^{\text{res}}(T, v) = a^{\text{mono}} + a^{\text{chain}} + a^{\text{assoc}}$ is the dimensionless residual term and $a^{\text{ideal}}(T, v) = a_0(T) - \ln(v/v_c)$ is the dimensionless ideal gas contribution. The critical part of the Helmholtz free energy $\Delta a(T, v)$, where $\Delta a(T, v) = a(T, v) - a_{\text{bg}}(T, v)$ is given by

$$\Delta a(\Delta T, \Delta v) = a^{\text{res}}(\Delta T, \Delta v) - a_0{}^{\text{res}}(\Delta T) - \ln(\Delta v + 1) + \Delta v\bar{P}_0(\Delta T) \quad (21)$$

where the background contribution $a_{\text{bg}}(T, v)$ is expressed as

$$a_{\text{bg}}(T, v) = -\Delta v\bar{P}_0(T) + a_0{}^{\text{res}}(T) + a_0(T) \quad (22)$$

In eqs 21 and 22, $\Delta T = T/T_{0c} - 1$ and $\Delta v = v/v_{0c} - 1$ are the dimensionless distances from the classical critical temperature (T_{0c}) and classical critical molar volume (v_{0c}), $a_0(T)$ is the dimensionless temperature-dependent ideal-gas term, and $\bar{P}_0(T) = P(T, v_{0,c})v_{0,c}/RT$ and $a_0{}^{\text{res}}(T) = a^{\text{res}}(T, v_{0,c})$ are the dimensionless pressure and residual Helmholtz free energy along the critical isochore, respectively. In the next step, we replace ΔT and Δv in the singular or critical part of the free energy, $\Delta a(\Delta T, \Delta v)$, with the renormalized values

$$\bar{\tau} = \tau Y^{-\alpha/2\Delta_1} + (1 + \tau)\Delta\tau_c Y^{2(2-\alpha)/3\Delta_1} \quad (23)$$

$$\bar{\varphi} = \varphi Y^{(\gamma-2\beta)/4\Delta_1} + (1+\varphi)\Delta v_c Y^{(2-\alpha)/2\Delta_1} \quad (24)$$

so that $\Delta T \rightarrow \bar{\tau}$ and $\Delta v \rightarrow \bar{\varphi}$ in eq 21. Here the superscripts correspond to the critical exponents, $\alpha = 0.112$, $\beta = 0.325$, and $\Delta_1 = 0.51$, $\tau = T/T_c - 1$ is the dimensionless deviation of the temperature from the real critical temperature T_c, $\varphi = v/v_c - 1$ is the dimensionless deviation of the molar volume from the real critical molar volume v_c, $\Delta\tau_c = \Delta T_c/T_{0c} = (T_c - T_{0c})/T_{0c}$ and $\Delta v_c = \Delta v_c/v_{0c} = (v_c - v_{0c})/v_{0c}$ are the dimensionless shifts of the critical parameters, and $Y(q)$ is the crossover function (specified below). In order to complete the transformation of the analytical thermodynamic potential $a(T, v)$ into the crossover form, one also needs to include the kernel term[40] in eq 21

$$K(\tau, \varphi) = \frac{1}{2}a_{20}\tau^2[Y^{-\alpha/\Delta_1} - 1] + \frac{1}{2}a_{21}\tau^2[Y^{-(\alpha-\Delta_1)/\Delta_1} - 1] \quad (25)$$

which is responsible for the asymptotic singular behavior of the isochoric heat capacity C_v along the critical isochore ($\Delta\varphi = 0$ at $\tau > 0$)

$$C_v(\tau)/R = -\frac{T}{R}\left(\frac{\partial^2 A}{\partial T^2}\right)_{\varphi=0} = A_0^{\pm}|\tau|^{-\alpha}(1 + a_1^{\pm}|\tau|^{+\Delta_1}) + B_0^{\pm}(\tau) \quad (26)$$

where $A_0^{\pm}$ is the asymptotic amplitude, $a_1^{\pm}$ is the first Wegner-correction term, and $B_0^{\pm}(\tau)$ is the background contribution above (+) and below (−) the critical temperature. Since the isochoric heat capacity is not considered in this work, we set $a_{20} = a_{21} = 0$ and, thus, do not include the Kernel term.

For the crossover function $Y(q)$ we use the simple phenomenological expression obtained by Kiselev et al.[41,42,45]

$$Y(q) = \left(\frac{q}{1+q}\right)^{2\Delta_1} \quad (27)$$

where q is a renormalized distance to the critical point. The crossover function $Y(q)$ given by eq 27 coincides with the corresponding crossover function in the crossover Leung−Griffiths model obtained from the first order ϵ-expansion by Belyakov et al.[55] As in previous work,[45,46] the renormalized distance q is obtained from the solution of the crossover sine model (SM)

$$\left(q^2 - \frac{\tau}{Gi}\right)\left[1 - \frac{1}{4}\left(1 - \frac{\tau}{q^2 Gi}\right)\right] = b^2\left(\frac{\varphi[1 + v_1\varphi^2\exp(-10\varphi) + d_1\tau]}{Gi^{\beta}}\right)^2 Y^{(1-2\beta)/\Delta_1} \quad (28)$$

where v_1, d_1, and Gi are the system-dependent parameters, and $b^2 = 1.359$ is the universal linear-model parameter.[44−46] The term proportional to $d_1\tau$ in eq 28 corresponds to the rectilinear diameter of the coexistence curve, while the term proportional to $v_1\exp(-10\varphi)$ ensures that $Y = 1$ at the triple point, hence ensuring that the crossover is complete.

The final crossover expression for the thermodynamic potential $a(T, v)$ can be written in the form

$$a(T, v) = \Delta a(\bar{\tau}, \bar{\varphi}) - K(\tau, \varphi) - \Delta v\bar{P}_0(T) + a_0(T) \quad (29)$$

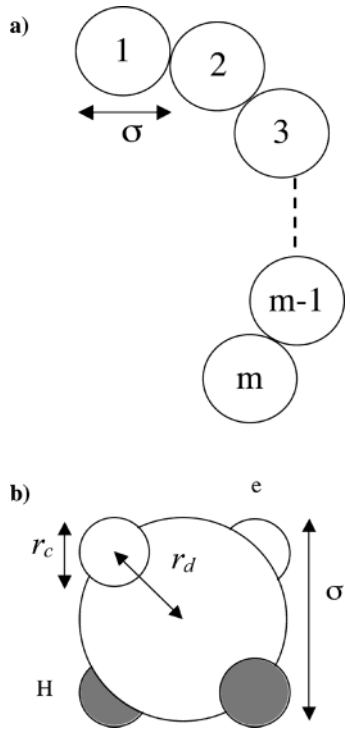

Figure 2. SAFT-VRX model for (a) *n*-alkanes and (b) water.

and the pressure obtained by differentiation of eq 29 with respect to volume

$$P(T, v) = -RT\left(\frac{\partial a}{\partial v}\right) = -\frac{RT}{v_{0c}}\left[\frac{v_{0c}}{v_c}\left\{\left(\frac{\partial \Delta a}{\partial \varphi}\right) + \left(\frac{\partial K}{\partial \varphi}\right)\right\} - \bar{P}_0(T)\right] \quad (30)$$

IV. Results

In this section we will present results for both associating and nonassociating fluids. In particular, we have studied the *n*-alkane homologous series for which we discuss the parametrization procedure followed in order to obtain simple expressions for the model parameters and allow the development of a predictive approach for other members of the homologous series. We then discuss the application of SAFT-VRX to associating and polar fluids. In particular, we present results for water and carbon dioxide.

In studying the *n*-alkane homologous series initially, we applied the SAFT-VRX EOS to selected (methane, ethane, and hexane) low molecular weight *n*-alkanes to assess the ability of the crossover model to accurately determine the thermodynamic properties.[56] In the SAFT-VR approach, the *n*-alkane molecules are described as chains of tangentially bonded hard spherical segments of diameter σ (Figure 2a) that interact through attractive interactions described by a square-well potential of variable range λ and depth ϵ (eq 6). Hence, in the description of nonassociating molecules, three parameters (σ, ϵ, and λ) are required to describe the strength of the molecular interactions, and an additional parameter m is used to determine the model chain length. The inclusion of the crossover function into the SAFT-VR equation of state introduces 3 additional parameters: the Ginzburg number Gi, the rectilinear diameter amplitude d_1, and an empirical coefficient v_1 related to the asymmetry of the vapor−liquid envelope.[44,57] Since the

Table 2. Coefficients in Equations 31−38 Which Define the SAFT-VRX Parameters for the *n*-Alkane Homologous Series

$a_{m,1}$	$6.62630348 \times 10^{-1}$	$a_{\epsilon,3}$	$-2.23873902 \times 10^{-1}$
$a_{m,2}$	$3.33333333 \times 10^{-1}$	$a_{g,0}$	7.87235801×10^{0}
$a_{\lambda,0}$	1.53051719×10^{0}	$a_{g,1}$	$-3.86985360 \times 10^{-1}$
$a_{\lambda,1}$	$1.03349047 \times 10^{-1}$	$a_{g,2}$	$4.08044603 \times 10^{-2}$
$a_{\lambda,2}$	$-6.51709763 \times 10^{-3}$	$a_{v,0}$	3.02550589×10^{0}
$a_{\sigma,0}$	1.34217767×10^{0}	$a_{v,1}$	$7.05301915 \times 10^{-1}$
$a_{\sigma,1}$	$8.64397896 \times 10^{-1}$	$a_{v,2}$	2.57032584×10^{2}
$a_{\sigma,2}$	$8.77979912 \times 10^{-3}$	$a_{d,0}$	$4.35059604 \times 10^{-1}$
$a_{\sigma,3}$	$-7.92051205 \times 10^{-2}$	$a_{d,1}$	$1.13282543 \times 10^{-2}$
$a_{\sigma,4}$	$5.68916683 \times 10^{-2}$	δ_η	2.08642177×10^{0}
$a_{\epsilon,0}$	3.30153122×10^{1}	C^{λ}_{max}	7
$a_{\epsilon,1}$	2.46011207×10^{1}	C^{ϵ}_{max}	28
$a_{\epsilon,2}$	3.13841789×10^{0}	δ_τ	0

goal of this initial study was to evaluate the ability of the SAFT-VRX equation to describe the thermodynamic properties of selected light hydrocarbons, all the parameters were determined by fitting to fluid property data, such as the vapor pressure curve, critical constants, coexisting densities, and PVT behavior. From this study, we were able to conclude that the SAFT-VRX EOS brings a drastic improvement in the description of the PVT and VLE surface of pure fluids in the critical region compared to SAFT-VR. For example, the accuracy of the SAFT-VRX equation of state in describing the coexisting densities of methane is demonstrated in Figure 1. Here the phase envelope obtained from the SAFT-VRX, SAFT-VR[21] (using both the original and rescaled parameters), and crossover HR-SAFT[41] equations of state are compared with experimental data. From the figure we note the overprediction of the critical point using the SAFT-VR equation of state and how the critical region is now correctly described using the crossover SAFT-VR approach, SAFT-VRX. However, we see from the figure that while the crossover version of SAFT-HR accurately describes the critical region, significant deviations from experimental data are seen at lower temperatures and pressures. This result emphasizes the fact that an accurate classical equation of state is essential for accurately reproducing the whole fluid phase diagram.

While this preliminary study demonstrated that SAFT-VRX can accurately describe the phase behavior of low molecular weight alkanes both in and far beyond the critical region, additional parametrization is needed to study the *n*-alkane homologous series. Rather than fit each alkane to available experimental data, the goal of this work is to develop a predictive SAFT-VRX EOS for the *n*-alkane homologous series by obtaining simple relations for the SAFT-VRX parameters that will enable the estimation of parameters without fitting to experimental data and for molecules for which no experimental data is available. With this goal in mind, we restricted the fitting process to a limited number of *n*-alkane molecules, namely ethane−hexane, octane, decane, eicosane, triacontane, and tetracosane. From the simultaneous optimization of the SAFT-VRX EOS to the VLE and PVT data for the ethane−hexane, octane, and decane and PVT data for eicosane, triacontane, and tetracosane, we obtained the following expressions

$$m = 1 + a_{m,1}(C_m - 1)^{0.1} + a_{m,2}(C_m - 1) \quad (31)$$

$$\lambda = a_{\lambda,0} + a_{\lambda,1}(C_m - 1)^{0.25} + a_{\lambda,2}(C_m - 1) \quad (32)$$

$$m\sigma = a_{\sigma,0} + a_{\sigma,1}(m\mathrm{Mw})^{0.5} + a_{\sigma,2}\left(\frac{m\mathrm{Mw}}{1 + a_{\sigma,4}C_m}\right) + a_{\sigma,3}\left(\frac{m\mathrm{Mw}}{1 + a_{\sigma,4}C_m}\right)^{0.75} \quad (33)$$

$$m\epsilon = a_{\epsilon,0} + a_{\epsilon,1}(m\mathrm{Mw})^{0.5} + a_{\epsilon,2}(m\mathrm{Mw})^{0.75} + a_{\epsilon,3}(m\mathrm{Mw}) \quad (34)$$

where C_m is the number of carbon atoms in the *n*-alkane chain, Mw the molecular weight, and $a_{x,i}$ fitted coefficients where $x = m$, σ, ϵ, or λ. Similar relations were obtained for the inverse Ginzburg number $g = 1/Gi$ and all other crossover parameters

$$g = a_{g,0} + a_{g,1}(C_m) + a_{g,2}(C_m)^{1.5} \quad (35)$$

$$v_1 = \frac{a_{v,0} + a_{v,1}C_m}{1 + a_{v,2}C_m} \quad (36)$$

$$d_1 = a_{d,0} + a_{d,1}C_m \quad (37)$$

$$\Delta v_c = -\frac{\delta_\eta Gi}{1 + Gi} \quad (38)$$

$$\Delta \tau_c = -\frac{\delta_\tau Gi}{1 + Gi} \quad (39)$$

Note two additional parameters are presented here, δ_η and δ_τ, which are coefficients used in the shift of the critical volume and critical temperature, respectively. During the optimization process, we found that the coefficient δ_τ for the critical temperature shift is statistically irrelevant, and therefore, for simplicity we fixed $\delta_\tau = 0$, thus setting in SAFT-VRX for *n*-alkanes the condition that $T_c \equiv T_{c,0}$, i.e., the experimental value. Had we also fixed the critical density to the experimental value we could further reduce the number of fitted parameters; however, we would not be able to use the SAFT-VRX EOS to predict the critical point of fluids for which experimental data does not exist. As a result, we choose to retain δ_η. We also found that if the parameters in eqs 32−34 are considered as free parameters, λ and ϵ rapidly approach limiting values with increasing carbon number, while σ tends to a limiting value more slowly. Additionally, we observed the coefficient $a_{m,2}$ to be very close to $^1/_3$, which is widely used in the prescription for m when applying the SAFT EOS to *n*-alkanes (i.e., $m = {}^1/_3(C - 1) + 1$).[17,27,58] Therefore, to restrict the number of the adjustable parameters and improve the predictability of the model we set $a_{m,2} = {}^1/_3$. The parameters in eqs 31−38 were then reoptimized, with the physical condition that λ and ϵ become constant once the limiting value is reached and $a_{m,2} = {}^1/_3$. The resulting coefficients for eqs 31−38 are listed in Table 2, and in Figures 3 and 4 we plot the parameters obtained as a function of carbon number C_m. As one can see from the figures, with the exception of the Ginzburg number, which passes through a maximum at $C_m \approx 40$ and then, in agreement with the theoretical prediction,[69] tends to zero at $C_m \to \infty$, all other coefficients are monotonic functions of C_m. In previous work with the SAFT-VR equation[27] it was found that for the *n*-alkane homologous series the classical SAFT-VR parameters σ, ϵ, and λ approached limiting values with increasing carbon number. From the simple linear relations determined

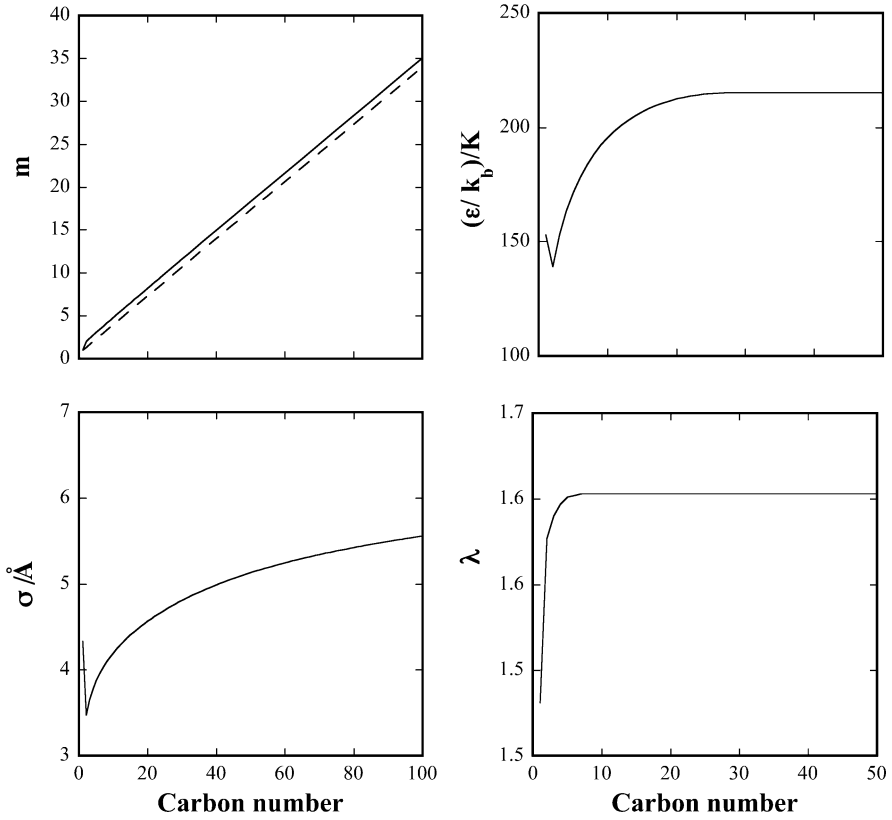

Figure 3. Behavior of the classical SAFT-VRX parameters for *n*-alkanes as a function of carbon number.

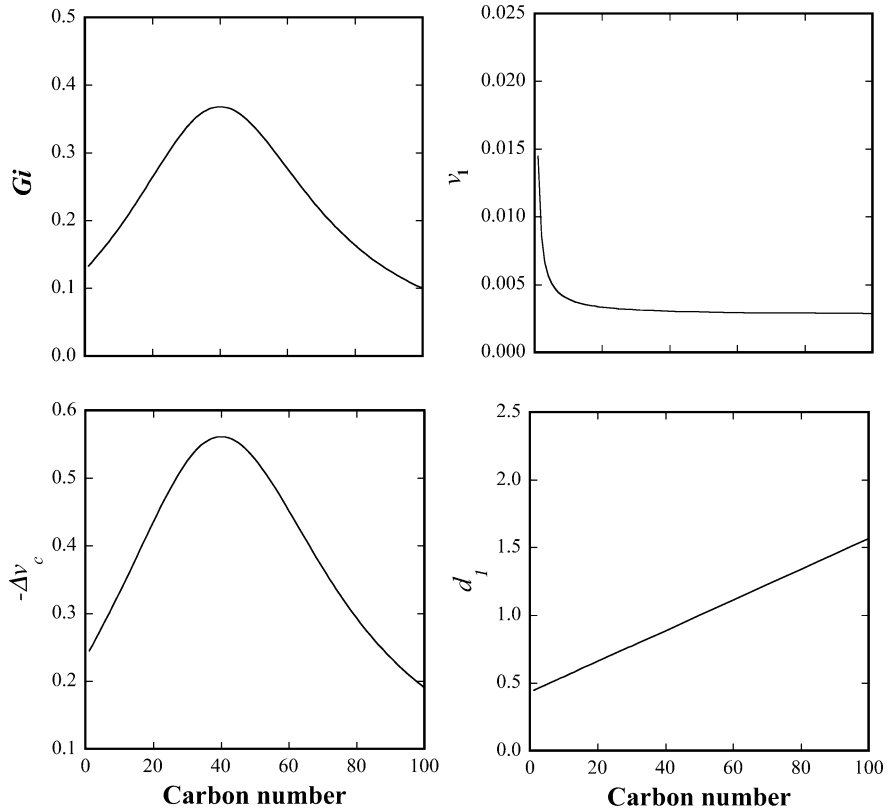

Figure 4. Behavior of the crossover SAFT-VRX parameters for *n*-alkanes as a function of carbon number.

for the model parameters as a function of molecular weight, the following limiting values are obtained: $\sigma \cong$ 4.0 Å, $\epsilon/k \cong$ 265 K, and $\lambda \cong 1.6$. For SAFT-VRX the plateau values are $\epsilon/k \cong$ 215 K, $\lambda = 1.653$ (reached at $C_m^{\epsilon} \geq 28$ and $C_m^{\lambda} \geq 7$ respectively), and $\sigma \cong 7$ Å, which for ϵ and λ are quiet similar to those observed for SAFT-VR. Although the hard core diameter is larger for SAFT-VRX than that observed in SAFT-VR, we believe this is more physical when one considers the size of a CH_2 group and the fact that a single segment in the SAFT model corresponds to ~3 carbon atoms. For example, in united atom models for the *n*-alkanes the diameter

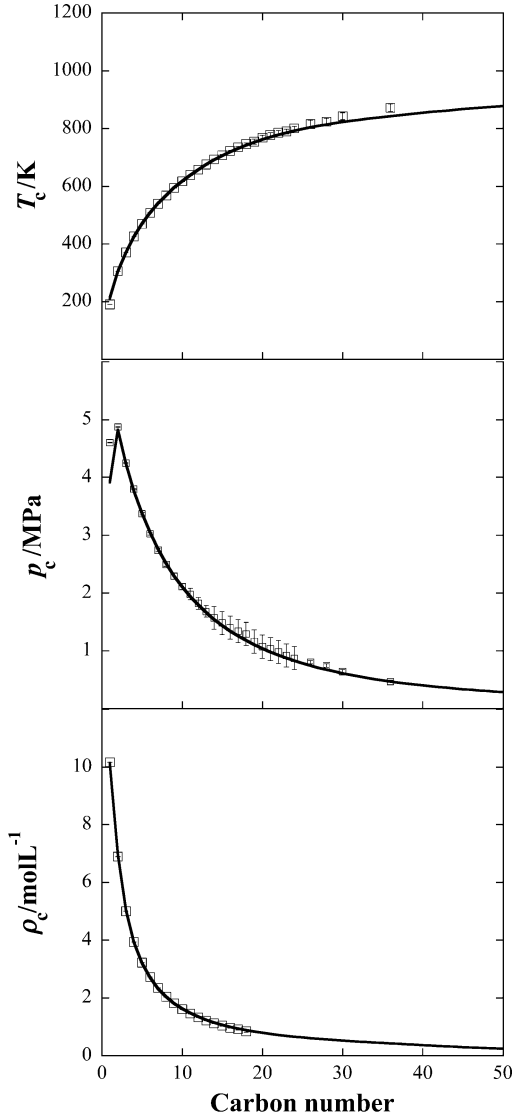

Figure 5. Critical parameters for the *n*-alkane homologous series as predicted by the SAFT-VRX EOS and compared with experimental data.[75]

of the CH_2 site is typically ~3.9−4.0 Å;[59−62] one would therefore expect the segment diameter in a more coarse grained model to be larger. Additionally, the asymptotic behavior of the parameter m at $C_m \rightarrow \infty$ practically coincides with the widely used expression in the SAFT approach for the number of model segments of *n*-alkane chains;[17,27,58] $m = 1 + (C_m - 1)/3$. Using the relations proposed in eqs 31−38, we will now examine the ability of SAFT-VRX to describe the thermodynamic properties of *n*-alkane molecules.

In Figure 5 we show the critical constants for the *n*-alkanes from methane through to C_{50} calculated with the SAFT-VRX EOS compared with experimental data. Excellent agreement between the theoretical predictions and experimental data for the critical constants is acheived, which provides a good test of the accuracy of our simple relations in determining the SAFT-VRX parameters for *n*-alkanes, particularly those not included in the fitting process. In Figure 6 we compare the experimental saturated vapor pressures for methane through to octane with the SAFT-VRX result. From the figure, we can see that excellent agreement is obtained with the experimental data both near to and far from the critical region. We should note that the SAFT-VRX

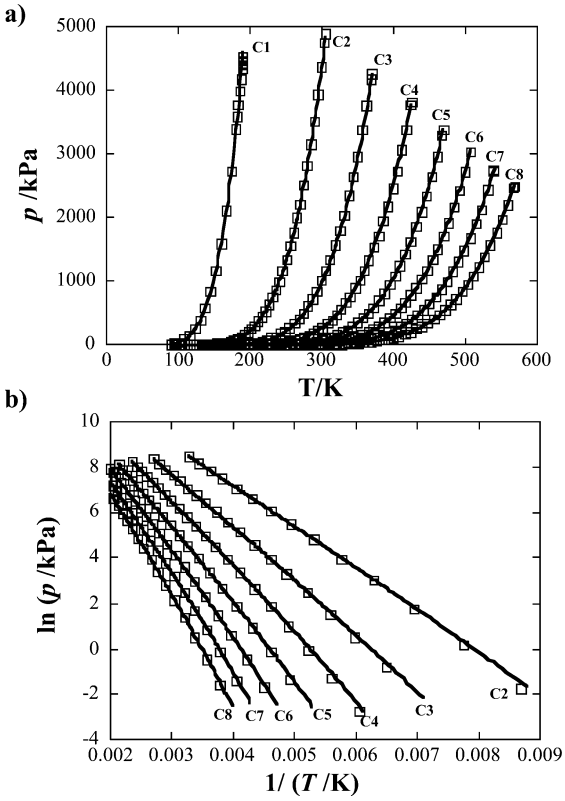

Figure 6. Vapor pressures of methane through *n*-octane. The symbols represent experimental data,[74] and the solid lines (—) the SAFT-VRX predictions.

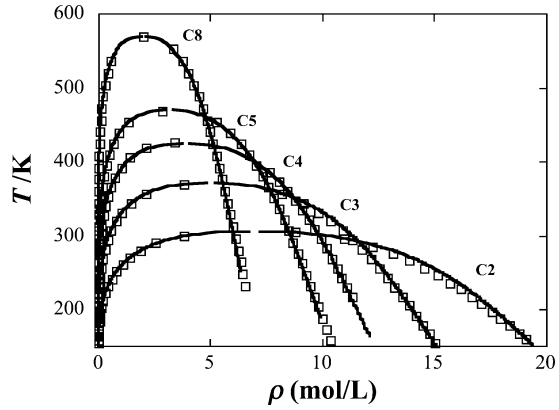

Figure 7. Coexisting liquid and gas densities for ethane, propane, *n*-butane, *n*-pentane, and *n*-octane. The symbols represent experimental data,[74] and the solid lines (—) the SAFT-VRX predictions.

description of the phase diagrams was obtained from the prescriptions for the potential model parameters given by eqs 31−38. Furthermore, the result for *n*-heptane is a pure prediction since *n*-heptane was not included in the fitting process. The coexisting densities for selected light *n*-alkanes as predicted from the SAFT-VRX equation of state and compared to experimental data are presented in Figure 7. Again, excellent agreement is achieved between the SAFT-VRX description and experiment.

Having seen that the relationships developed for the potential model parameters can accurately describe the fluid phase diagrams of the light *n*-alkanes, which would be anticipated given that ethane−hexane and octane were included in the fitting process, we now turn to the heavier alkanes. In Figure 8 we compare the coexisting densities and vapor pressure curves for selected *n*-

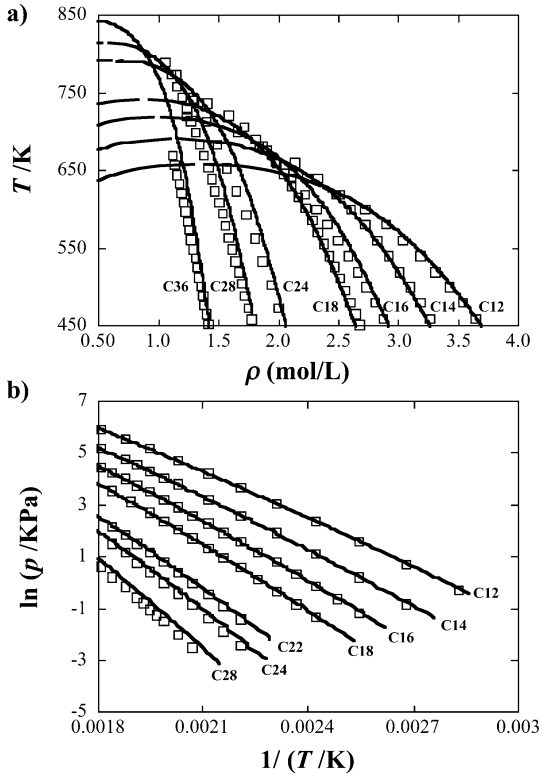

Figure 8. (a) Saturated liquid densities and (b) vapor pressure curves for dodecane (C_{12}), tetradecane (C_{14}), hexadecane (C_{16}), octadecane (C_{18}), tetracosane (C_{24}), octacosane (C_{28}), and hexatriacontane (C_{36}). The symbols represent experimental data,[63,76,77] and the solid lines (—) the SAFT-VRX predictions.

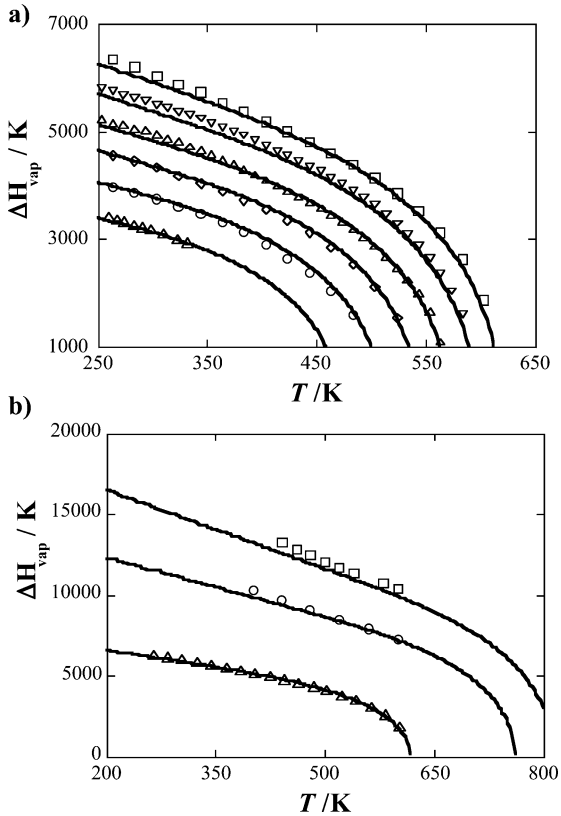

Figure 9. Enthalpy of vaporization for (a) pentane, hexane, heptane, octane, nonane, and decane (from the inner curve to the outer curve) and (b) decane, eicosane, and octacosane (from the inner curve to the outer curve). The symbols represent experimental data,[63,77] and the solid lines (—) the SAFT-VRX predictions.

alkanes from C_{12} to C_{36} with experimental data. From the figures, we can see excellent agreement between the theoretical predictions and experimental data, particularly for the shorter chains. For the longer chains, we notice some disagreement between the SAFT-VRX description and experiment. However, we note that this is seen for *n*-alkanes for which it is difficult to make experimental measurements and significant disagreements arise between different sets of experimental data. In Figure 9 we compare the enthalpy of vaporization predicted from the SAFT-VRX EOS, again using the proposed relations to determine the parameters for each *n*-alkane, with experimental data.[63] These comparisons represent true predictions for all the molecules considered since no data on the enthalpy of vaporization were included in the fitting process for any alkane.

We now examine the PVT behavior. In Figures 10 and 11 we present predictions from the SAFT-VRX equation of state compared with experimental data over a range of state conditions for selected *n*-alkanes (nonane, undecane, heptadecane, and tetracosane). We note that PVT data for nonane, undecane, and heptadecane were not included in the fitting process. In all cases excellent agreement with experimental data is observed further confirming the accuracy of SAFT-VRX in predicting the thermodynamic properties of both short and long chain *n*-alkanes.

We now consider the ability of the SAFT-VRX EOS to describe the phase behavior of other nonassociating as well as associating fluids, namely, carbon dioxide and water. Water is described as a hard sphere of diameter σ with four embedded, off-center, square-well bonding sites (see Figure 2b). Two of the bonding sites account for the electron lone pairs (e) and two for the hydrogen atoms (H) of the water molecule; only e−H bonding is

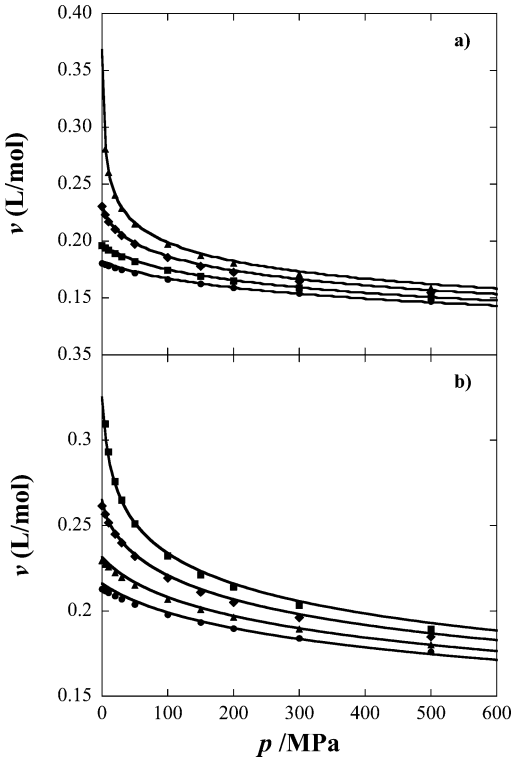

Figure 10. PVT isotherms for (a) nonane at ● 303 K, ■ 373 K, ◆ 473 K, and ▲ 573 K and (b) undecane at ● 303 K, ■ 373 K, ◆ 473 K, and ▲ 573 K. The symbols represent experimental data,[78] and the solid lines (—) the SAFT-VRX predictions at each temperature.

allowed. The sites are placed a distance $r_d = 0.25\sigma$ from the center of the hard core and have a cutoff range r_c;

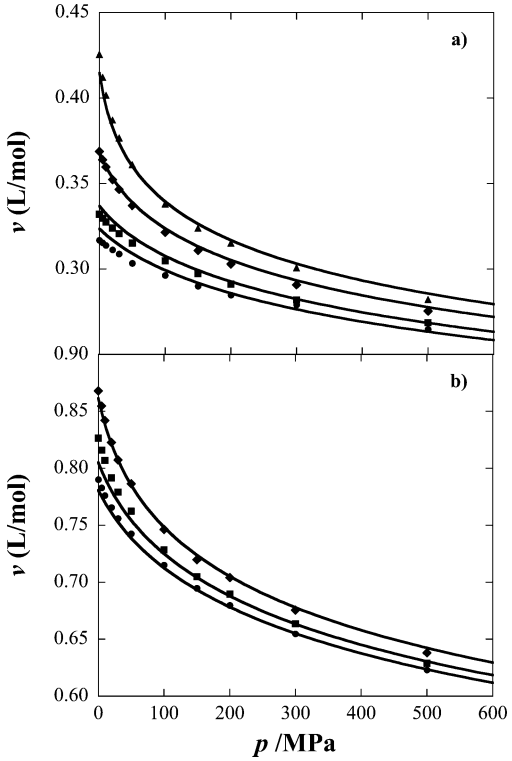

Figure 11. PVT isotherms for (a) heptadecane at ● 323 K, ■ 373 K, ◆ 473 K, and ▲ 573 K and (b) for tetracontane at ● 473 K, ■ 523 K, and ◆ 573 K. The symbols represent experimental data,[78] and the solid lines (—) the SAFT-VRX predictions at each temperature.

when the distance between e and H sites is less than r_c, a site−site attractive interaction energy ϵ_{HB} occurs. This is intended to mimic the short-range directional hydrogen-bonding interactions that dominate the physical properties of aqueous systems. The corresponding bonding volume can be determined from the range and position of the bonding site by

$$K = \frac{4\pi\sigma^2}{72r_d^2}\left[\ln\left(\frac{(r_c + 2r_d)}{\sigma}\right) \times \frac{(6r_c^3 + 18r_c^2r_d - 24r_d^3)}{\sigma^3} + \frac{(r_c + 2r_d - \sigma)(22\sigma r_d^2 - 5\sigma r_c r_d - 7r_d - 8\sigma r_c^2 + \sigma^2 r_c + \sigma^3)}{\sigma^3}\right] \quad (40)$$

As for the *n*-alkanes the dispersion interaction between water molecules is modeled via a square-well potential of range λ and depth ϵ. Following the work of Blas and Galindo,[64] we model CO_2 as nonassociating and nonspherical. Although CO_2 has a significant quadrupole moment, we do not include the quadrupole explicitly, but in an effective way via the square-well potential. For both CO_2 and water, the model parameters were determined by fitting to saturated liquid densities, vapor pressures, and PVT data in the one-phase region. For the critical temperature and density for water, we adopt the values recommended by IAPWS[65] (T_c = 647.096 K, ρ_c = 322.0 kg/m^3) and for carbon dioxide the values reported by Duschek et al.[66] (T_c = 314.136 K, ρ_c = 467.6) kg/m^3. The model parameters are listed in Table 3, along with parameters taken from the literature for SAFT-VR. For water we see that the hard-core diameter for SAFT-VRX is larger than the value used in SAFT-VR; however, the larger value is in keeping with simulation

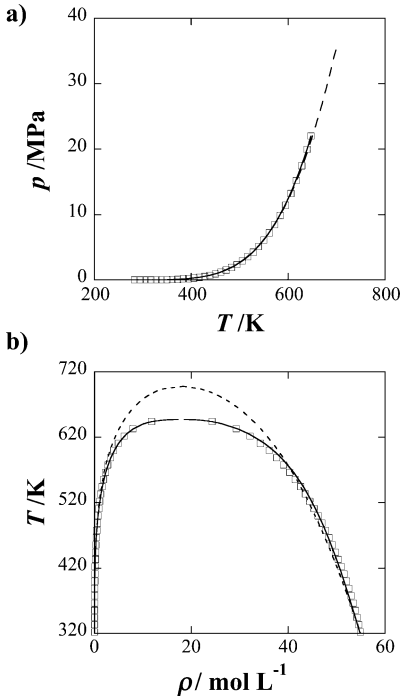

Figure 12. (a) Vapor pressure curve and (b) coexisting densities for carbon dioxide. The symbols represent experimental data,[66] the solid line (—) the predictions of the SAFT-VRX equation, and the dashed line (- - -) predictions from the SAFT-VR equation.

Table 3. SAFT-VRX and SAFT-VR[64,68] Parameters for Water and Carbon Dioxide

	H_2O		CO_2	
	VRX	VR	VRX	VR
m	1.00000000×10^0	1.00	2.69072802×10^0	2.00
σ, Å	3.41184330×10^0	3.036	2.72242917×10^0	2.7864
λ	2.39403902×10^0	1.80	1.62483581×10^0	1.5257
ϵ/k_B, K	5.22989133×10^1	253.3	1.24115027×10^2	179.27
ϵ_{HB}/k_B, K	1.90896088×10^3	1366		
κ, Å^3	1.02319970×10^0	1.028		
g	2.46395973×10^0		5.95079659×10^0	
v_1	$6.70420940 \times 10^{-3}$		$5.70122746 \times 10^{-3}$	
d_1	$5.72105128 \times 10^{-1}$		$8.22826137 \times 10^{-1}$	
δ_η	1.08648565×10^0		1.84701671×10^0	
δ_τ	$4.31990535 \times 10^{-2}$		$2.27572970 \times 10^{-2}$	

models for water.[67] The magnitude of the attractive potential for carbon dioxide obtained for SAFT-VRX is very similar to that used in SAFT-VR. However, for water this quantity is found to be weaker in SAFT-VRX than in SAFT-VR, while the strength of the hydrogen-bonding interactions are stronger. In Figures 12 and 13, we compare the vapor pressure curves and saturated coexisting densities obtained from the SAFT-VRX equation for carbon dioxide and water, respectively. For comparison, we have also included in the figures the SAFT-VR description of the phase behavior.[64,68] For these complex and associating fluids, we see significant improvement compared to the SAFT-VR description and excellent agreement between SAFT-VRX and experimental data, both in and far from the critical region. A more extensive study of other complex and associating fluids and their mixtures will be presented in a future publication.

V. Discussion

We have developed a crossover SAFT equation of state, SAFT-VRX, which accurately describes the fluid

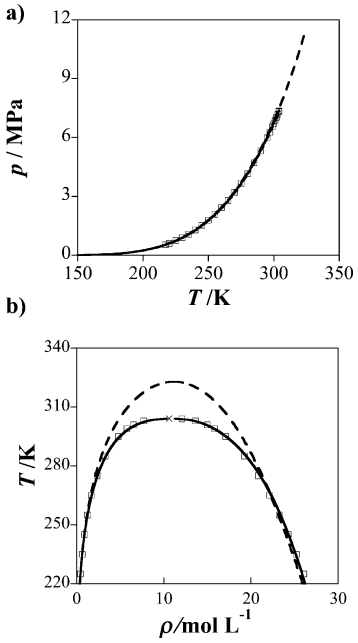

Figure 13. (a) Vapor pressure curve and (b) coexisting densities for water. The symbols represent experimental data,[65] the solid line (—) the predictions of the SAFT-VRX equation and the dashed line (- - -) predictions from the SAFT-VR equation.

phase behavior both in and far from the critical region by combining the SAFT-VR equation with the crossover function of Kiselev.[40] The SAFT-VRX equation exhibits the correct nonanalytical, singular behavior exhibited by real fluids, enabling the accurate description of the whole phase diagram with a single set of parameters. The results presented here for the *n*-alkane homologous series are seen to be in excellent agreement with experimental data both near to and far from the critical region. Results were also presented for water and carbon dioxide illustrating the accuracy of the SAFT-VRX approach when applied to more complex, associating, and polar fluids. Additionally, by fitting to selected *n*-alkanes, we have developed simple relations for the SAFT-VRX parameters that enable the estimation of parameters for the *n*-alkane homologous series without fitting to experimental data and for molecules for which no experimental data are available. The molecular rather than empirical nature of the SAFT EOS allows the development of such relations, which can then be used confidently in a predictive sense.

In Figure 14, the critical compressibility factor for the *n*-alkanes from methane through to C_{50} calculated with the SAFT-VRX EOS is presented and compared with experimental data. The dotted curve in the figure describes the phenomenological expression for Z_c obtained for a fluid composed of long chain molecules by Lue et al.[69] This expression was determined from the condition that the virial coefficients B_i scale correctly with the chain molecular weight in the long chain limit, i.e., $B_i \propto (C_m)^{3(i-2)/2}$. As one can see from Figure 14, the critical compressibility factor calculated by Lue monotonically decreases and reaches a value of $Z_c \approx 0.18$ for infinitely long chains. We note that the values calculated with the SAFT-VRX EOS, for which $B_i \propto (C_m)^i$, first decrease in accordance with theoretical prediction by Lue et al., but then pass through a minimum at $C_m \approx 45$ and tend to the classical value of $^1/_3$ as $C_m \rightarrow \infty$ ($C_m^{-1/2} \rightarrow 0$). To correctly describe this behavior for $C_m \rightarrow \infty$, the correct renormalization of the virial coefficients at

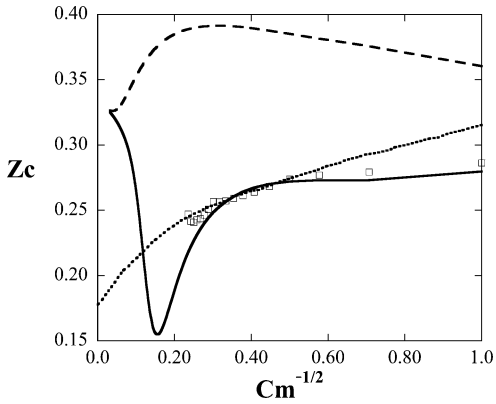

Figure 14. Critical compressibility factor for the *n*-alkanes. The symbols represent experimental data,[75] the solid line (—) the predictions of the SAFT-VRX equation, the dashed line (- - -) predictions from the classical SAFT-VR equation, and the dotted curve (···) correspond to the values calculated by Lue et al.[69]

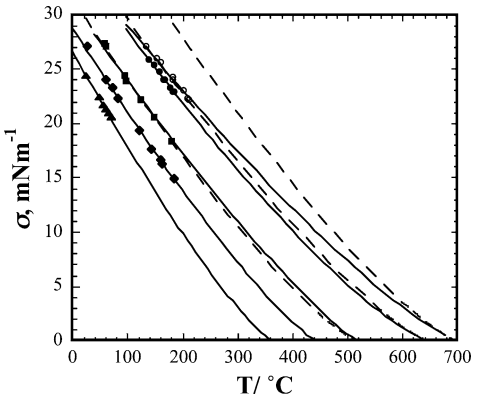

Figure 15. Surface tension data for *n*-decane (▲), hexadecane (◆), tetracosane (■), *n*-C_{78} (●), n-C_{150} (○). The symbols represent experimental data,[79] the solid lines (—) the predictions of the SAFT-VRX + DFT model, and the dashed lines (- - -) results from the model of Le Naindre and Garrabos.[73]

$C_m \rightarrow \infty$ should be also incorporated into the SAFT-VRX model. This issue becomes especially important in reproducing the universal scaling behavior of long chain polymer molecules in the dilute and semidilute regimes.[70] However, for *n*-alkanes this nonmonotonic behavior of Z_c appears in the region where no experimental data are available, and we see that, in its present form, the SAFT-VRX equation yields an excellent representation of the thermodynamic surface for the *n*-alkanes studied close in and far beyond the critical region.

As a final test of the predictability of the SAFT-VRX equation for the *n*-alkanes, we consider the surface tension of hydrocarbons up to C_{150}. In Figure 15 we show a comparison of experimental surface tension data with calculated values obtained by combining the SAFT-VRX equation with density functional theory. Within density functional theory the surface tension can be written in terms of the gradient of the density profile from[71]

$$\sigma = c_0^{1/2} \int_{\rho_v}^{\rho_l} [\Delta \hat{A}(\rho)]^{1/2} \, d\rho \qquad (41)$$

For the parameter c_0, we used an approximation developed in earlier work:[72] $c_0 = (1 - \kappa_0)^2 k T_0 \rho_c^{1/3}$, where the system dependent parameter κ_0 has been determined for each system from a single experimental surface tension data point at $T \cong 0.6 T_c$. The free-energy density for the vapor−liquid interface $\Delta\hat{A}$ given by

$$\Delta\hat{A} = \rho A(T, \rho) - \rho_v A(T, \rho_v) - (\rho - \rho_v)\mu(T) \quad (42)$$

where $\mu(T, \rho_{v,l}) = (\partial\rho A/\partial\rho)_\tau$ is the chemical potential of the bulk fluid along the saturation curve, $\rho = \rho_{v,l}(T)$, was calculated from the SAFT-VRX equation with parameters as given by eqs 31−38. The results of our calculations are presented in Figure 15 along with values calculated for C_{24}, C_{78}, and C_{150} from the empirical expression proposed by Le Naindre and Garrabos.[73] As one can see from the figure for the lower *n*-alkanes ($C_m \leq 24$), both models are essentially equivalent; however, with increasing carbon number ($C_m \geq 78$) the model by Naindre and Garrabos[73] exhibits significant deviations from experimental data, while the SAFT-VRX + DFT model is in excellent agreement with experimental data up to C_{150}. Furthermore, we find that for *n*-alkanes with $C_m \geq 70$ a simple linear expression can be used to determine the coefficient κ_0; $\kappa_0 = -0.36 - 0.01792(C_m - 78)$, which enables a true prediction of the surface tension since no experimental data is required.

Acknowledgment

C.M.C. acknowledges support from the NSF under Grant CTS-0319062 and the U.S. Department of Energy, Office of Basic Energy Sciences, under Grant DE-FG02-03ER15385. S.B.K. acknowledges the U.S. Department of Energy, Office of Basic Energy Sciences, under Grant DE-FG03-95ER14568. We also wish to thank Eric Whitebay for help with collecting experimental data.

List of Symbols

A = Helmholtz free energy per molecule
a = Helmholtz free energy per segment
d_1 = rectilinear diameter amplitude
Gi = Ginzburg number
k = Boltzmann constant
m = number of segments in model chain
N = number of molecules
n = total number of sites
p = pressure
T = temperature
u = square-well potential
v = molar volume
v_1 = crossover parameter in Y
Y = crossover function
y = cavity distribution function
X_a = fraction of molecules not bonded at site a
α = universal critical exponent for specific heat
β = universal critical exponent for the coexistence curve
ϵ = depth of square-well potential
γ = universal critical exponent for susceptibility
λ = width of square-well potential
ρ = number density
σ = hard core diameter
τ = reduced temperature difference
$\bar{\tau}$ = renormalized temperature difference
φ = order parameter
$\bar{\varphi}$ = renormalized order parameter
η = packing fraction
ideal = ideal-gas contribution
mono = monomeric contribution
assoc = association contribution
chain = chain contribution
res = residual
0 = classical
c = critical
r = reduced

Literature Cited

(1) Peng, D.; Robinson, D. B. *Ind. Eng. Chem. Fundam.* **1976**, *15*, 59−64.
(2) Redlich, O.; Kwong, J. N. S. *Chem. Rev.* **1949**, *44*, 233−244.
(3) Anderko, A. In *Equations of State for Fluids and Fluid Mixtures*; Sengers, J. V., Kayser, R. F., Peters, C. J., White, H. J., Eds.; Elsevier: Amsterdam, 2000; Vol. 1.
(4) Donohue, M. D.; Prausnitz, J. M. *AIChE J.* **1978**, *24*, 849−860.
(5) Beret, S.; Prausnitz, J. M. *AIChE J.* **1975**, *21*, 1123−1132.
(6) Ikonomou, G. D.; Donohue, M. D. *AIChE J.* **1986**, *32*, 1716−1725.
(7) Muller, E. A.; Gubbins, K. E. In *Equations of State for Fluids and Fluid Mixtures*; Sengers, J. V., Kayser, R. F., Peters, C. J., White, H. J., Eds.; Elsevier: Amsterdam, 2001; Vol. 1.
(8) Wertheim, M. S. *J. Stat. Phys.* **1984**, *35*, 19−34.
(9) Wertheim, M. S. *J. Stat. Phys.* **1984**, *35*, 35−47.
(10) Wertheim, M. S. *J. Stat. Phys.* **1986**, *42*, 459−476.
(11) Wertheim, M. S. *J. Stat. Phys.* **1986**, *42*, 477−492.
(12) Chapman, W. G.; Gubbins, K. E.; Jackson, G.; Radosz, M. *Fluid Phase Equilib.* **1989**, *52*, 31−38.
(13) Chapman, W. G.; Gubbins, K. E.; Jackson, G.; Radosz, M. *Ind. Eng. Chem. Res.* **1990**, *29*, 1709−1721.
(14) Muller, E. A.; Gubbins, K. E. *Ind. Eng. Chem. Res.* **2001**, *40*, 2193−2211.
(15) Chapman, W. G.; Jackson, G.; Gubbins, K. E. *Mol. Phys.* **1988**, *65*, 1057−1079.
(16) Jackson, G.; Chapman, W. G.; Gubbins, K. E. *Mol. Phys.* **1988**, *65*, 1−31.
(17) Galindo, A.; Whitehead, P. J.; Jackson, G.; Burgess, A. N. *J. Phys. Chem.* **1996**, *100*, 6781−6792.
(18) Galindo, A.; Whitehead, P. J.; Jackson, G.; Burgess, A. N. *J. Phys. Chem. B* **1997**, *101*, 2082−2091.
(19) Huang, S. H.; Radosz, M. *Ind. Eng. Chem. Res.* **1990**, *29*, 2284−2294.
(20) Huang, S. H.; Radosz, M. *Ind. Eng. Chem. Res.* **1991**, *30*, 1994−2005.
(21) Gil Villegas, A.; Galindo, A.; Whitehead, P. J.; Mills, S. J.; Jackson, G.; Burgess, A. N. *J. Chem. Phys.* **1997**, *106*, 4168−4186.
(22) Galindo, A.; Davies, L. A.; Gil-Villegas, A.; Jackson, G. *Mol. Phys.* **1998**, *93*, 241−252.
(23) McCabe, C.; Gil-Villegas, A.; Jackson, G. *J. Phys. Chem. B* **1998**, *102*, 4183−4188.
(24) McCabe, C.; Galindo, A.; Gil-Villegas, A.; Jackson, G. *J. Phys. Chem. B* **1998**, *102*, 8060−8069.
(25) McCabe, C.; Galindo, A.; Gil-Villegas, A.; Jackson, G. *Int. J. Thermophys.* **1998**, *19*, 1511−1522.
(26) Galindo, A.; Gil-Villegas, A.; Whitehead, P. J.; Jackson, G.; Burgess, A. N. *J. Phys. Chem. B* **1998**, *102*, 7632−7639.
(27) McCabe, C.; Jackson, G. *Phys. Chem. Chem. Phys.* **1999**, *1*, 2057−2064.
(28) Filipe, E. J. M.; de Azevedo, E.; Martins, L. F. G.; Soares, V. A. M.; Calado, J. C. G.; McCabe, C.; Jackson, G. *J. Phys. Chem. B* **2000**, *104*, 1315−1321.
(29) Filipe, E. J. M.; Martins, L. F. G.; Calado, J. C. G.; McCabe, C.; Jackson, G. *J. Phys. Chem. B* **2000**, *104*, 1322−1325.
(30) McCabe, C.; Galindo, A.; Garcia-Lisbona, M. N.; Jackson, G. *Ind. Eng. Chem. Res.* **2001**, *40*, 3835−3842.
(31) Scott, R. L.; Konynenburg, P. H. v. *Discuss. Faraday Soc.* **1970**, *49*.
(32) Sengers, J. V.; Levelt Sengers, J. M. H. *Ann. Rev. Phys. Chem.* **1986**, *37*, 189−222.
(33) Levelt Sengers, J. M. H.; Hocken, R.; Sengers, J. V. *Phys. Today* **1977**, *30*, 42.
(34) Belyakov, M. Y.; Kiselev, S. *Physica A* **1992**, *190*, 75−94.
(35) Sengers, J. V.; Kayser, R. F.; Peters, C. J.; White, H. J. *Equations of State for Fluids and Fluid Mixtures*; Elsevier: Amsterdam, 2000.
(36) Chapela, G. A.; Rowlinson, J. S. *J. Chem. Soc., Faraday Trans. 1* **1974**, *70*, 584−593.
(37) Albright, P. C.; Sengers, J. V.; Nicoll, J. F.; Leykoo, M. *Int. J. Thermophys.* **1986**, *7*, 75−85.
(38) Van Pelt, A.; Jin, G. X.; Sengers, J. V. *Int. J. Thermophys.* **1994**, *15*, 687−697.

(39) Wyczalkowska, A. K.; Anisimov, M. A.; Sengers, J. V. *Fluid Phase Equilib.* **1999**, *160*, 523−535.
(40) Kiselev, S. B. *Fluid Phase Equilib.* **1998**, *147*, 7−23.
(41) Kiselev, S. B.; Ely, J. F. *Ind. Eng. Chem. Res.* **1999**, *38*, 4993−5004.
(42) Kiselev, S. B.; Friend, D. G. *Fluid Phase Equilib.* **1999**, *162*, 51−82.
(43) Vanpelt, A.; Jin, G. X.; Sengers, J. V. *Int. J. Thermophys.* **1994**, *15*, 687−697.
(44) Kiselev, S. B.; Ely, J. F.; Abdulagatov, I. M.; Magee, J. W. *Int. J. Thermophys.* **2000**, *21*, 1373−1405.
(45) Kiselev, S. B.; Fly, J. F. *Fluid Phase Equilib* **2000**, *174*, 93−113.
(46) Kiselev, S. B.; Ely, J. F.; Adidharma, H.; Radosz, M. *Fluid Phase Equilib.* **2001**, *183*, 53−64.
(47) Hu, Z.-Q.; Yang, J.-C.; Li, Y.-G. *Fluid Phase Equilib.* **2003**, *205*, 25−36.
(48) Hu, Z.-Q.; Yang, J.-C.; Li, Y.-G. *Fluid Phase Equilib.* **2003**, *205*, 1−15.
(49) White, J. A.; Zhang, S. *Int. J. Thermophys.* **1998**, *19*, 1019−1027.
(50) White, J. A.; Zhang, S. *J. Chem. Phys.* **1993**, *99*, 2012−2019.
(51) Jiang, J. W.; Prausnitz, J. M. *J. Chem. Phys.* **1999**, *111*, 5964−5974.
(52) Jiang, J. W.; Prausnitz, J. M. *AIChE J.* **2000**, *46*, 2525−2536.
(53) Jiang, J. W.; Prausnitz, J. M. *Fluid Phase Equilib.* **2000**, *169*, 127−147.
(54) Patel, B.; Varga, S.; Galindo, A.; Maitland, G. C. *Mol. Phys.*, in preparation.
(55) Belyakov, M. Y.; Kiselev, S. B.; Rainwater, J. C. *J. Chem. Phys.* **1997**, *107*, 3085−3097.
(56) McCabe, C.; Kiselev, S. B. *Fluid Phase Equilib.* **2004**, *219* (1), 3−9.
(57) Kiselev, S. B.; Ely, J. F. *Fluid Phase Equilib.* **2000**, *174*, 93−119.
(58) Jackson, G.; Gubbins, K. E. *Pure Appl. Chem.* **1989**, *61*, 1021−1026.
(59) Smit, B.; Karaborni, S.; Siepmann, J. I. *J. Chem. Phys.* **1995**, *102*, 2126−2140.
(60) Martin, M. G.; Siepmann, J. I. *J. Phys. Chem. B* **1998**, *102*, 2569−2577.
(61) Errington, J. R.; Panagiotopoulos, A. Z. *J. Phys. Chem. B* **1999**, *103*, 6314−6322.
(62) Nath, S. K.; Escobedo, F. A.; de Pablo, J. J. *J. Chem. Phys.* **1998**, *108*, 9905−9911.
(63) Vargaftik, N. B. *Handbook of Physical Properties of Liquids and Gases: Pure Substances and Mixtures*, 2nd ed.; Springer-Verlag: Berlin, 1983.
(64) Blas, F. J.; Galindo, A. *Fluid Phase Equilib.* **2002**, *194*−*197*, 501−509.
(65) "Release of the IAPWS Formulation 1995 for the Thermodynamic Properties of Ordinary Water Substance for General and Scientific Use," Available from the IAPWS Executive Secretary: Dr. R. B. Dooley, Electric Power Research Institute, 3412 Hillview Ave., Palo Alto, CA 94304, 1996.
(66) Duschek, W.; Kleinrahm, R.; Wagner, W. *J. Chem. Thermodyn.* **1990**, *22*, 841−864.
(67) Chialvo, A. A.; Cummings, P. T. *Adv. Chem. Phys.* **1999**, *109*, 115−205.
(68) Galindo, A.; Gil-Villegas, A.; Jackson, G.; Burgess, A. N. *J. Phys. Chem. B* **1999**, *103*, 10272−10281.
(69) Lue, L.; Friend, D. G.; Elliott, J. R. *Mol. Phys.* **2000**, *98*, 1473−1477.
(70) Lue, L. *J. Chem. Phys.* **2000**, *112*, 3442−3449.
(71) Davis, H. T. *Statistical Mechanics of Phases, Interfaces, and Thin Films*; Wiley: New York, 1995.
(72) Kiselev, S. B.; Ely, J. F. *J. Chem. Phys.* **2003**, *119*, 8645−8660.
(73) Le Neindre, B.; Garrabos, Y. *Fluid Phase Equilib.* **2002**, *198*, 165−183.
(74) Smith, B. D.; Srivastava, R. *Thermodynamic Data for Pure Compounds*; Elsevier: London, 1986.
(75) Nikitin, E. D. *High Temp.* **1998**, *36*, 305−318.
(76) *DIPPR 801 Tables*; Design Institute for Physical Property Data: Provo, UT, 1992.
(77) Chirico, R. D.; Nguyen, A.; Steele, W. V.; Strube, M. M. *J. Chem. Eng. Data* **1989**, *34*, 149−156.
(78) Doolittle, A. *J. Chem. Eng. Data* **1964**, *9*, 275−279.
(79) Dee, G. T.; Sauer, B. B. *Adv. Phys.* **1998**, *47*, 161−205.

Received for review December 7, 2003
Revised manuscript received February 25, 2004
Accepted March 4, 2004

IE034288N